PSYCHOMETRIKA—VOL. 76, NO. 1, 124–152
JANUARY 2011
DOI: 10.1007/S11336-010-9194-0

A NETWORK APPROACH FOR EVALUATING COHERENCE IN MULTIVARIATE SYSTEMS: AN APPLICATION TO PSYCHOPHYSIOLOGICAL EMOTION DATA

FUSHING HSIEH AND EMILIO FERRER

UNIVERSITY OF CALIFORNIA, DAVIS

SHUCHUN CHEN

ACADEMIA SINICA

IRIS B. MAUSS

UNIVERSITY OF DENVER

OLIVER JOHN

UNIVERSITY OF CALIFORNIA, BERKELEY

JAMES J. GROSS

STANFORD UNIVERSITY

We present an approach for evaluating coherence in multivariate systems that considers all the variables simultaneously. We operationalize the multivariate system as a network and define coherence as the efficiency with which a signal is transmitted throughout the network. We illustrate this approach with time series data from 15 psychophysiological signals representing individuals' moment-by-moment emotional reactions to emotional films. First, we summarize the time series through nonparametric Receiver Operating Characteristic (ROC) curves. Second, we use Spearman rank correlations to calculate relationships between each pair of variables. Third, based on the obtained associations, we construct a network using the variables as nodes. Finally, we examine signal transmission through all the nodes in the network. Our results indicate that the network consisting of the 15 psychophysiological signals has a small-world structure, with three clusters of variables and strong within-cluster connections. This structure supports an effective signal transmission across the entire network. When compared across experimental conditions, our results indicate that coherence is relatively stronger for intense emotional stimuli than for neutral stimuli. These findings are discussed in relation to multivariate methods and emotion theories.

Key words: multivariate analysis, dynamical systems, time series, emotion

1. Definition and Measurement of Coherence

Many psychological theories use the term coherence to describe the coordination of responses associated with a given stimulus. In emotion research, for example, theorists have postulated that emotions involve a coordination of experiential, behavioral, and physiological responses, as the emotion unfolds over time (e.g., Ekman, 1972, 1992; Lazarus, 1991; Levenson, 1994, 2003; Matsumoto, Nezlek, & Koopmann, 2007; Scherer, 1984; Tomkins, 1962). However,

This study was supported in part by grants from the National Science Foundation (BCS-05-27766 and BCS-08-27021) and NIH-NINDS (R01 NS057146-01).

Requests for reprints should be sent to Emilio Ferrer, Department of Psychology, University of California, Davis, Davis, CA 95616-8686, USA. E-mail: eferrer@ucdavis.edu

Analytic Step	*Technique*	*Description – Objective*
Step 1	Receiver Operating Characteristic Curve (*ROC*) Spearman rank correlations	Examine differences among segments in each time series, determining a rank order of discrepancies among segments Determine relationship between pairs of variables for each individual
Step 2	Simulation	Compute multivariate matrix with proportion of individuals with relationships between each pair of variables
Step 3	Hierarchical Clustering	Examine the distribution of distances among the variables Identify clusters of variables with strong associations and those with weaker links
Step 4	Stochastic Transition Networks (*STN*)	Develop a stochastic network with connections between variables based on probabilities from Step 2 Examine the transmission of a signal across all the nodes in the network

FIGURE 1.
Description and goals of the different analytic steps.

strong empirical support for this hypothesis is lacking. More generally, almost all research concerning coherence has relied upon pairwise analyses of two variables, and not much evidence is available that considers coherence as a system-wise measure that includes multiple variables simultaneously (cf. P-technique factor analysis, Cattell, Cattell, & Rhymer, 1947; and dynamic factor analysis, e.g., Browne & Nesselroade, 2005).[1]

One possible reason for this gap between theory and empirical work is the lack of adequate methodology for constructing a dynamic system that considers all sampled variables. Ideally, this construction would involve techniques for analyzing multiple time series simultaneously, especially with series of different metrics and waveforms, as is often the case in emotion data. In this paper, we propose an approach to examine system-wise coherence among all the variables comprising a dynamic system. We illustrate our approach with data consisting of 15 time series of experiential, behavioral, and physiological emotion measures.

The present article is organized according to the analytic steps that we propose. We first describe ROC curve analysis and Spearman rank correlations as a joint approach to measure pairwise coherence. Our goal in this step is to determine relationships between variables within each individual. In Step 2, we combine this information across all individuals in a multivariate matrix representing proportions of individuals with significant relationships between each pair of variables. In Step 3, we use hierarchical clustering to examine the distribution of distances among all variables and identify clusters of variables. In Step 4, we develop a stochastic network with connections between variables based on the probabilities in Step 2. We examine signal transmission across all the nodes in the network as a measure of system-wise coherence. A description of these analytic steps is presented in Figure 1.

To illustrate these steps, we apply our proposed method to psychophysiological data. Guiding our methodology and analytic steps are a number of theoretical questions. First, we would like

[1]These techniques can be used to analyze multivariate time series data, providing information on the underlying structure. Although different from our approach, this information could be used to examine coherence.

to examine whether—and under what conditions—there is a coordination of various emotion responses, our measure of coherence. Second, we want to examine whether such coherence varies with the valence of the situation (i.e., positive and negative—amusing and sad situations—cf. Feldman-Barrett, 2006). Finally, we want to investigate what are the connections among emotion variables (e.g., physiological, behavioral, experiential) that lead to a coordinated pattern of responses. We examine such connections in terms of a network, and the coordination in terms of signal transmission in the network.

2. Foundations of System-Wise Coherence in Multivariate Systems

2.1. *Assessing Pairwise Coherence*

2.1.1. ROC Curve Analysis A fundamental question in the social and behavioral sciences is the identification of patterns of time-varying responses. In psychological research, such associations between variables are typically assessed using cross-correlations (e.g., Gottman, 1990; Mauss, Levenson, McCarter, Wilhelm, & Goss, 2005) and are the common approach to infer coherence. Although potentially informative (e.g., Brillinger, 2001), and useful to examine lagged relations (e.g., Boker, Xu, Rotondo, & King, 2002), cross-correlations are not robust and, under certain conditions (e.g., time series with different measurement units and intrinsic waveforms), might lead to inaccurate inferences. To avoid such possible shortcomings of cross-correlations we turn to more robust nonparametric approaches.[2] In particular, we propose using Spearman rank correlations together with ROC curves (Hsieh & Turnbull, 1996) to build a network of associations among multiple variables. ROC curves have been used extensively in signal detection theory as a tool to discriminate between signal and noise (for a review, see Swets, 1996).

In most data distributions, the mean value is less informative than the distribution itself. Time series of emotion variables, for example, could show intermittency (i.e., interruption or periodic stopping) and specific waveforms (e.g., sine wave), and such frequency changes are likely to appear in their corresponding distributions. Thus, a reasonable way to compare two variables and, especially, their associations is using their distributions via ROC curves (Hsieh & Turnbull, 1996). Several steps are needed for this. First, a given time series is represented in terms of its distribution. Second, the time series is partitioned into segments according to some criteria (e.g., experimental stimuli) and a distribution is derived from each of the resulting segments. Third, using ROC curves, the distribution of each segment is compared with the distribution of the entire series, resulting in ROC areas.

Figure 2 represents ROC curves for two distributions $F(x)$ and $G(x)$, where $F(x)$ is the reference distribution. If both distributions have similar shape and $G(x)$ is located to the left of $F(x)$, then the ROC curve is concave upward and is located under the diagonal line (panel (a)). In this case, the random variable corresponding to $F(x)$ is stochastically larger (i.e., higher mean for the distribution) than the random variable corresponding to G_1. If, however, $G_2(x)$ is located to the right of $F(x)$, then the ROC curve is concave downward and is located above the diagonal line (panel (b)). If the two distributions are significantly different, as $F(x)$ and $G_3(x)$ in panel (c), then the ROC curve could cross the diagonal line. The larger the ROC area (in absolute value), the farther apart the two distributions are, indicating differences between the two variables. In particular, for an empirical ROC curve $1 - \hat{G}(\hat{F}^{-1}(1-t))$, its area is computed as:

$$A[R] = \int_0^1 1 - \hat{G}\big(\hat{F}^{-1}(1-t)\big)\,dt.$$

[2] Appendix A includes a simulation illustrating differences between cross-correlations and Spearman rank correlations under different data conditions.

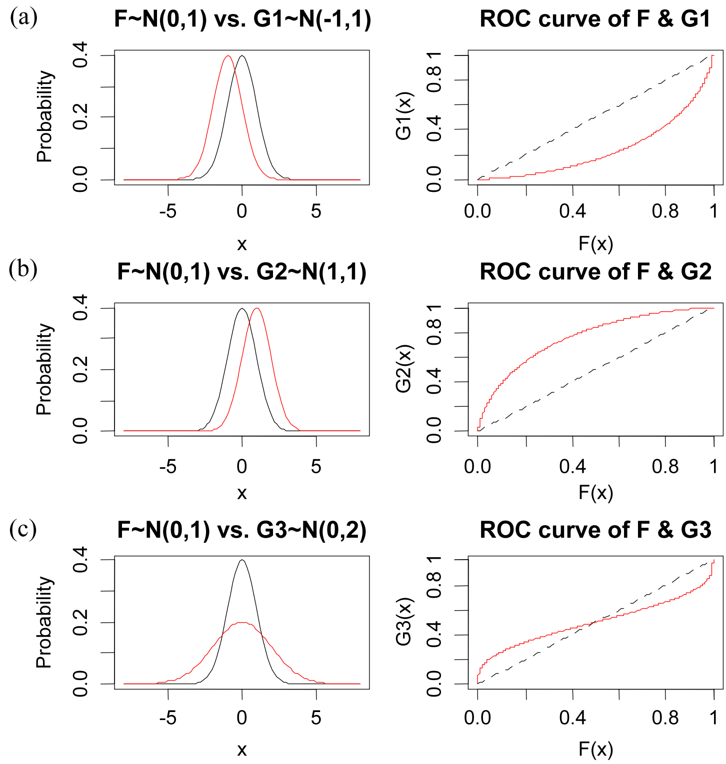

FIGURE 2.
ROC curves for the distributions $F(x)$ and $G(x)$ under various differences in mean and variance. The $F(x)$ distribution is $N(0, 1)$ in the *first column* and the diagonal line in the *second column*.

Because the empirical ROC curve is a stepwise function, the integration is a finite sum.

In sum, for each segment in the series, the ROC curve analysis results in a measure that represents the distance between the segment's curve and the curve from the entire series. The larger this measure, the more the segment differs from the overall pattern. We will use these ROC areas to represent differences between variables across individuals.

2.1.2. From ROC Curves to Spearman Correlations Let $X^{(j)}$ and $A^{(j)}$ be, respectively, the entire time series and the sequence of ROC curve areas derived from the jth variable, with $j = 1, \ldots, J$ for a single individual. The Spearman rank correlation (SRC) coefficient $\hat{\rho}(j, j')$ between $A^{(j)}$ and $A^{(j')}$ is computed as the sample correlation of $O^{(j)}$ and $O^{(j')}$, where O indicates a sequence of ranking among K segments in the time series. Because the correlations are based on the rankings among the segments in the time series, they represent the extent to which two time series co-vary in the way their various segments are ranked. Given that the rankings reflect the departure of the distribution of each segment from that of the overall series, the correlation represents a linear association of the distributions of the various segments across the two time series. If, for example, the various segments represent experimental tasks with stimuli that elicit different responses, two time series can show signals that differ across the tasks but follow a similar pattern across the series. This coherence between both time series would be reflected in the Spearman-correlations that we use in our approach.

Under the null hypothesis of zero correlation and with $K < 30$, the symmetric distribution of $\hat{\rho}(j, j')$ can be found in tables (see, e.g., Rohatgi, 1984). If $K = 12$ (as in our empirical illustration) the resulting probability is $P[\hat{\rho}(j, j') > 0.503] = 0.05$. When $K \geq 30$, we can use asymptotic nonparametric results—under the null hypothesis of zero correlation—as $\sqrt{K-1}\hat{\rho}(j, j')$ approaches a standard normal distribution; that is, $\sigma^2(\hat{\rho})_0 = \text{Var}[\hat{\rho}(j, j')|\rho(j, j') = 0] \approx \frac{1}{K-1}$.

2.2. *From Spearman Correlations to a Multivariate Network*

Given the distributional results of $\hat{\rho}(j, j')$, we can use the computed correlations for each person to evaluate whether two variables are correlated in the population. That is, for each pair of variables, we estimate the proportion of correlations across all individuals that exceeds a threshold value. Because the Type-I error probability (e.g., 0.05) corresponds to a threshold value (e.g., 0.503, for $K = 12$) pertaining to the distribution of the computed correlation, such proportion can be taken as the probability of having a non-zero correlation in the population. Such proportion can also be thought as indicating the strength of association between the two variables in the population.[3]

These values are then used to build a network connecting all the variables. Each node in the network represents one variable and the wiring among all nodes represents the association among all variables in the system. In particular, we use the calculated proportion for each pair of variables as the probability that the corresponding nodes are linked. We then use the pattern of connections among all the nodes as a measure of system-wise coherence.

More formally, we can define our network as follows. For any individual m, the SRC coefficient $\hat{\rho}^{(m)}(j, j')$ on any (j, j') pair of variables is used to test the null hypothesis $H_0 : \rho^{(m)}(j, j') = 0$. If the significance level is set at α, then the critical value for a one-sided test can be calculated using the exact distribution of the Spearman rank statistic. For example, given $\alpha = 0.05$ and $K = 12$, then the critical value is 0.503. If $|\hat{\rho}^{(m)}(j, j')| > 0.503$, we conclude that observing such an extreme correlation is unlikely under the null hypothesis.[4]

Thus, for a collection of computed correlation coefficients, denoted as $\{\hat{\rho}^{(m)}(j, j')\}_{m=1}^{M}$ for the (j, j') pair of variables, we can compute the following proportion

$$\hat{p}(h|j, j') = \max\left\{\sum_{m=1}^{M} 1_{\{\hat{\rho}^{(m)}(j,j')>h\}}, \sum_{m=1}^{M} 1_{\{\hat{\rho}^{(m)}(j,j')<-h\}}\right\} \Big/ M \tag{1}$$

with regard to any threshold value h; where the "max" statement is used here to accommodate both negative and positive correlations. This proportion is a reasonable estimate of the probability of finding a "non-zero" correlation between the (j, j') pair of variables in the population for a significance $\alpha(h)$ level. Repeating this computation for all possible pairs among the J variables yields a symmetric $J \times J$ matrix with diagonal elements as zero and off-diagonal entries specified by the collection of $J(J-1)/2$ values of $\hat{p}(h|j, j')$. This $\mathcal{P}(h)$ matrix is used to construct a network by linking all connections of (j, j') pairs of variables with probability $\hat{p}(h|j, j')$.

An example of a network is depicted in Figure 3. Here, each node represents a hypothetical variable. In this network, the connection between any two nodes can be stochastically established

[3] For each pair of variables measured on each individual, we consider a hypothesis testing of zero correlation (H_o) against a non-zero correlation (H_a). We denote a 0–1 random variable Y_i as the binary result of this testing, so that $Y_i = 1$ if the ith subject's correlation exceeds the critical value 0.503 with respect to the nominal level 0.05; otherwise, $Y_i = 0$. We assume that the collection of results $\{Y_i\}_{i=1}^{n}$ for all n subjects is representative of the corresponding population pertaining to the pair of variables. With this definition, we have probability $Pr[Y_i = 1|H_o] = 0.05$. In contrast, $Pr[Y_i = 1|H_a]$ is the power of the test statistic of the correlation under H_a.

[4] Given the defined probabilities $Pr[Y_i = 1|H_o] = 0.05$ and $Pr[Y_i = 1|H_a]$, we make the theoretical assumption that individuals in this population are uniform in that they either show or do not show correlation for each pair of variables. Given this uniformness as well as mutual independence among all individual tests, the Law of Large Numbers predicts that the average $1/n \sum_{i=1}^{n} Y_i = \bar{Y}_n$ should be close to 0.05 if H_o is true in the population. If, however, $\bar{Y}_n$ is far away from 0.05, then the pair of variables is more likely correlated via the classic argument based on n Bernoulli random variables. In that case, the population likely follows H_a and $\bar{Y}_n$ should be taken as the empirical estimate of the power.

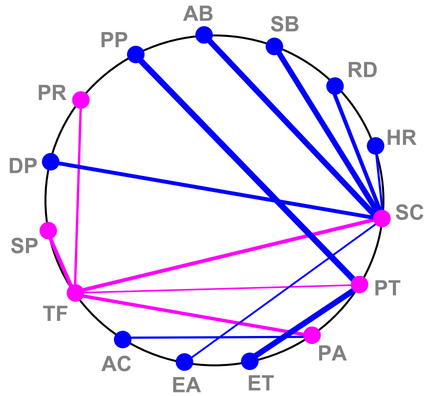

FIGURE 3.
Small-world network of emotion coherence. Nodes represent variables (see Table 1 for variable labels and description) and paths between nodes represent connections between pairs of variables at the first time step (*pink*) or second time step (*blue*) after an initial signal in a randomly selected node (TF).

with a computed probability at each time step (i.e., each time the signal is transmitted from one node to its connected neighbors) as described in the preceding paragraphs. For example, the pink and blue colors in this figure represent first and second time steps, respectively. We can use this network as a representation of a multivariate dynamic system comprising a set of emotion-related variables.

Consider, for example a network in which the nodes represent neurons and the edges indicate whether or not they are connected. Consider also a network representing people, with the edges indicating whether or not they know each other. Our empirical data consist of psychophysiological variables. Thus, our network represents the structure of relationships among psychophysiological variables, with each node representing a psychophysiological variable. The edges indicate the probability of association between each pair of psychophysiological variables. Variables that represent a similar process (e.g., cardiac activity) might be more strongly associated with each other than with variables that represent a different process (e.g., facial behavior versus cardiac activity). These patterns of associations are reflected in the structure of the network

2.3. *Adding Stochastic Components to the Multivariate Network*

Based on the probability $\hat{p}(h|j, j')$, we establish a wiring between nodes j and j'. For this, we generate a uniform [0, 1] random variable $U_{jj'}$ that is compared with the probability $\hat{p}(h|j, j')$. If $U_{jj'} < \hat{p}(h|j, j')$, the nodes j and j' connect; otherwise, they remain unconnected. We repeat this random wiring for all $J(J-1)/2$ pairs of nodes in the system. The goal of this procedure is to create a network in which the connections—based on probabilities of associations between variables and the total number of possible connections—are unlikely to exist by chance. This procedure yields a stochastic network ($\mathcal{SN}$) with a number of expected connections $N_W(h) = \sum_{j<j'} \hat{p}(h|j, j')$. Again, this network represents a multivariate system in which the associations among pairs of variables are reflected in the edges. Furthermore, such associations are based on the obtained empirical associations, thus representing the strength of connectedness between the two variables in the population. Using the probabilities of such connections as distances between variables, hierarchical clustering is performed to examine the distribution of distances among all variables. This technique (see, e.g., Hastie, Tibshirani, & Friedman, 2009; Johnson, 1967) is used to identify groups of variables that cluster together with the goal of building a hierarchy of such clusters. The resulting structure can be visualized using hierarchical trees (or dendrograms). Those variables with strong associations will cluster together in the same

branch, whereas those with weaker links will be located in different branches (more details are provided in subsequent sections).

Among the expected connections in the stochastic network, the number that are likely to be false is estimated by $F_W(h) = \alpha(h)N_W(h)$. Ideally, this number of false wirings should be as small as possible. In reality, however, $F_W(h)$ cannot be too small because it would increase the threshold value h and would make the number of expected connections $N_W(h)$ smaller. Such a network with very sparse wiring would likely have many isolated nodes or independent small clusters of nodes, not revealing much structure of the system. The goal, hence, is to find a balance between the ratio of false to expected wirings and the amount of information revealed by the network. One aspect of this balance can be achieved in probabilistic terms, evaluating the likelihood that a dynamic pattern with expected $N_W(h)$ wirings is due to possible false $F_W(h)$ wirings.

Imagine, for instance, a network with many redundant wirings. In this network, not all the connections are indispensable and the removal—or failure—of some wirings does not affect the network's overall behavior, thus making it a robust network. A well-known example of such type of robust structure is the small-world network (Watts, 1999). Small-world networks are structures that were first proposed to describe human friendship networks and acquaintance connection (Milgram, 1967), and have been used to characterize social networks (Amaral, Diaz-Guilera, Mareira, Goldberger, & Lipsitz, 2004), collaboration graph of film actors, the power grid of the western United States (Watts & Strogatz, 1998), or the world wide web (Albert, Jeong, & Barabási, 1999). Applications in psychology are almost non-existent (cf. Tsonis & Tsonis, 2004, for an example on memory).

A small-world structure is characterized by several clusters of nodes, with connections among the clusters. This structure allows all the nodes in the network to be reachable within a small number of steps, even if they are located in distant points of the network. Such structure is effective for transferring and processing information throughout the network while maintaining strong stability and associations within the clusters. This overall connectedness would be difficult to identify with measures of pairwise associations.

In our application, we examine whether the interrelations among the psychophysiological variables can be characterized as a small-world network. We use the connection of all the variables as a measure of coherence in the system. Our proposed network is a stochastic version of the small-world network in which the connections are expressed in probabilistic terms.

2.4. Efficiency of Signal Transmission Within the Stochastic Network

Once the network is constructed, coherence among all the variables in the system can be measured. For this, we define coherence as the efficiency with which a signal is transmitted among all the nodes in the network. We compute efficiency of signal transmission at each discrete time step as the cumulative proportion of nodes in the network that are activated by a signal originated from a randomly selected node. Our criterion for system-wise coherence is the number of time steps required to reach a stable configuration (i.e., no more nodes can be activated). The fewer the number of time steps (for a fixed number of nodes), the higher the coherence in the system. To quantify this, we conduct a Monte Carlo simulation with 10,000 replications and a newly constructed network at each replication (as described in the previous section) and examine the proportion of nodes activated at each step.

Consider the networks depicted in Figure 4. All the networks are comprised of nine nodes but with different configurations. The efficiency of signal transmission in any stochastic network $\mathcal{SN}$ is a computed expectation of the proportion of activated nodes at each time step (as in McAssey, Hsieh, & Ferrer, 2010). For example, Network A is fully connected. Given the activation of any node in this network, it would take only one step to transmit the signal to all

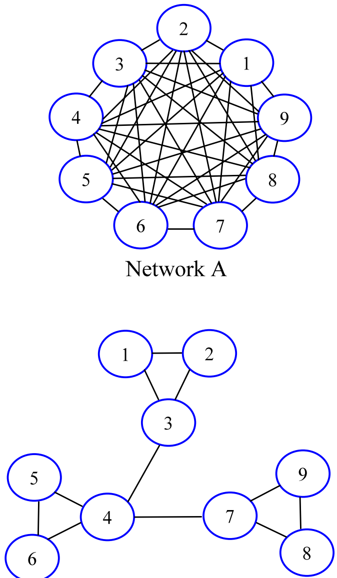

	Number of Steps Until Network is Completely Activated								
	Initial Node								
Network	1	2	3	4	5	6	7	8	9
A	3	3	3	3	3	3	3	3	3
B	4	4	3	3	4	4	3	4	4
C	5	5	5	4	4	4	5	5	5
D	5	5	4	5	6	7	5	6	7

FIGURE 4.
Signal transmission in networks.

remaining nodes. Networks B–D, in contrast, are comprised of several clusters with slightly different connecting structure. Network B has three fully connected clusters, which themselves are also interconnected. Network C is similar to B but one of the connections among the clusters is missing. In Network D the clusters are interconnected but the nodes in each cluster are not fully connected. In Networks B–D, the node where the signal originates is now relevant when computing efficiency in signal transmission. Similarly, the absence of certain connections between nodes within and across subsystems results in an increase of the number of steps needed to activate all nodes in the network. Appendix B includes an algebraic representation of the described networks and their signal transmission.

To clarify, the time steps in this approach refer to steps needed to achieve a state of system-wise coherence, or coordination among all the variables. They do not directly reflect time in the metric of the time series or represent lagged relationships. Similarly, signal transmission is related to degree of association among the variables. Consider, for example, the activation of certain variables in our system (e.g., as a response to a given stimulus). At this first step, those variables will connect with other variables to which they are more strongly related, based on the computed proportions in the population. Variables not related will remain unconnected. The first step represents such initial connections. The next time step represents the next opportunity for variables to connect (e.g., time needed for a physiological transmission, new experimental condition). At this step, the new set of variables that reached connection are now allowed to connect with their neighbors (i.e., those to which they are strongly related), and so on.

In other words, the time steps in our approach represent the structure of association among all the variables in the network. Given that such connections are based on a probability threshold, computed from all possible connections, these time steps represent the extent to which the variables in the system are connected. A network that requires many steps to reach system-wise coherence would be one in which the variables are loosely associated. In the following sections, we illustrate the described analytic procedure with empirical data.

3. Empirical Illustration: System-Wise Coherence in Emotional Responses

3.1. Participants

Participants were 151 (48% female) undergraduate students who were participating in a larger project. The mean age of the sample was 21.1 years (SD = 0.6) and the ethnic composition was mixed: 2% African American, 30% Asian American, 43% European American, 9% Latino American, 11% of multiple ethnic background, and 5% other or unknown. Written informed consent was obtained after the procedures had been fully explained, and participants were paid for their participation.

3.2. Procedure

The data consist of emotion responses from an experimental setting. Participants watched a nine-minute film clip that was composed of an amusing, a neutral, a sad, and another neutral segment (each segment was approximately two minutes long). Three different groups of films were presented—but always in the order of amusing, neutral, sad, neutral; and participants were randomly assigned to one of them (denoted as A, B and C). All segments had been pretested to primarily evoke the target emotion (cf. Rottenberg, Ray, & Gross, 2007), and intensity of target emotions was matched across the three types. Measures of experience, behavior, and autonomic physiological responses were obtained during the film clips. Time series for each variable for one individual are presented in Figure 5. The different colors in these plots correspond to the four film segments (i.e., amusement, neutral, sadness, neutral).

3.3. Measures

3.3.1. Continuous Ratings of Emotion Experience During the film, participants were instructed to rate their emotion experience using a rating dial similar to that used by Levenson and Gottman (1983; see also Gottman & Levenson, 1985). The dial consisted of a pointer that could be moved along a 180° scale, with the legends "extremely sad" at 0° and "extremely amused" at 180°. It was attached to a potentiometer in a voltage dividing circuit, which yielded near continuous data (1000 Hz).

3.3.2. Continuous Ratings of Emotion Behavior Coders rated second-to-second facial expressions of amusement and sadness from video recordings of participants' faces. The coding system was informed by microanalytic analyses of expressive behavior (Ekman & Friesen, 1978), and was anchored at 0 with neutral (no sign of emotion) and 8 with strong laughter for amusement and strong sadness expression/sobbing for sadness. Average inter-rater reliabilities were satisfactory, with Cronbach's alphas = 0.89 (SD = 0.13) for amusement behavior and 0.79 (SD = 0.11) for sadness behavior. We thus averaged the coders' ratings to create one second-by-second amusement and one second-by-second sadness rating for each participant.

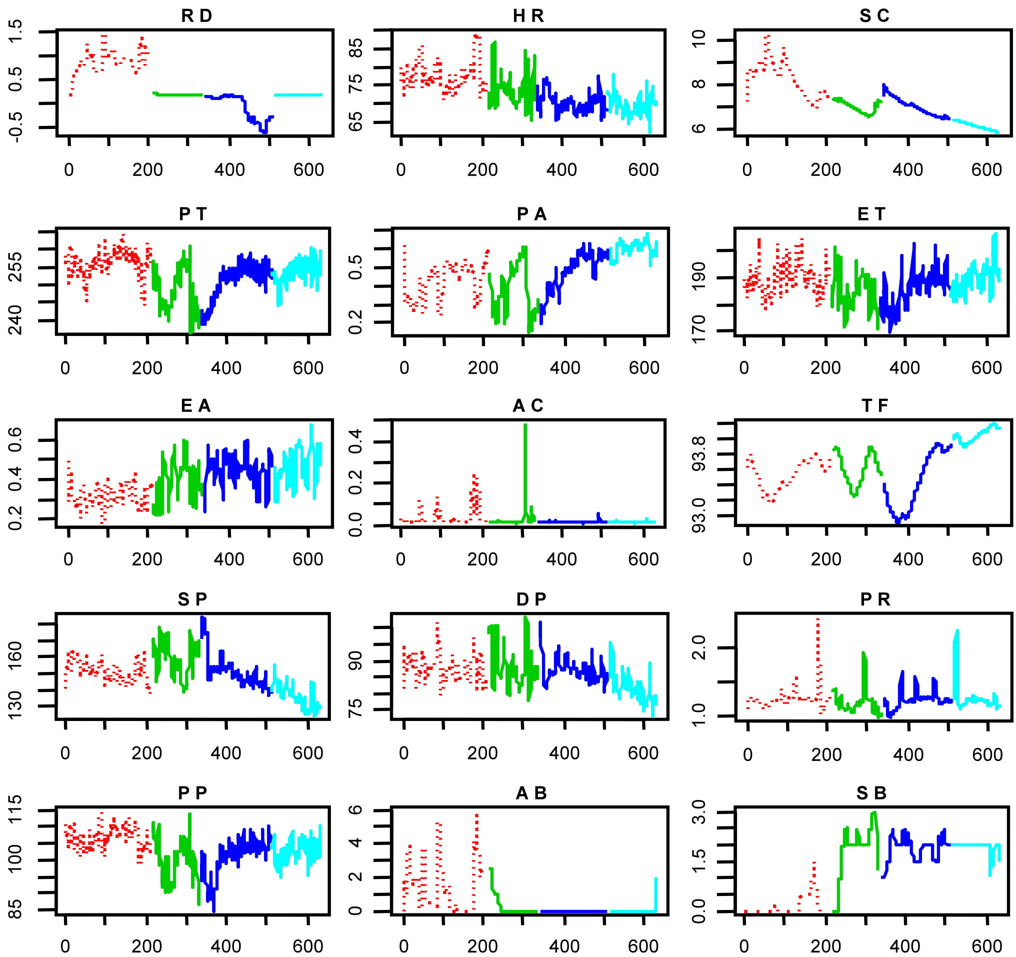

FIGURE 5.
Observed time series data from all 15 variables for one individual. Colors correspond to the different films (*red* = amusement; *green* = neutral; *blue* = sadness; *cyan* = neutral), the X-axis represents time (in seconds), and the Y-axis represents the variable score (see Table 1 for variable labels and description).

3.3.3. Continuous Measures of Autonomic Physiology During the film, physiological measures were sampled at 1000 Hz using laboratory software. 12 measures representing cardiovascular, electrodermal, and somatic activation were obtained, including heart rate, finger and ear pulse amplitude, finger and ear pulse transit time, finger temperature, systolic and diastolic blood pressure, total peripheral resistance, pre-ejection period, skin conductance level, and somatic activity. For a full description of the physiological equipment and the specific measurement constructs, see Mauss and colleagues (Mauss et al., 2005; Mauss, Evers, Wilhelm, & Gross, 2006). A list of all the variables used in this study is in Table 1.

3.4. Step 1: ROC Areas and Spearman Rank Correlations

In the first step of analyses (see Figure 1), we transformed each of the $J = 15$ time series from each individual into a string of digital ranking and computed ROC areas. To transform the time series, we first considered the four segments corresponding to the four films. Each segment was then partitioned into three additional fractions, which yielded a string of rankings

TABLE 1.
Emotion measures.

Continuous Ratings of Emotion Experience
RD = Rating dial (unpleasant—pleasant)
Continuous Ratings of Emotion Behavior
AB = Facial amusement behavior
SB = Facial sadness behavior
Continuous Measures of Autonomic Physiology
HR = Heart rate
PT = Finger pulse transit time
PA = Finger pulse amplitude
ET = Ear pulse transit time
EA = Ear pulse amplitude
TF = Finger temperature
SP = Systolic blood pressure
DP = Diastolic blood pressure
PR = Total peripheral resistance
PP = Pre-ejection period
SC = Skin conductance level
AC = Somatic activity

from 1 to 12. This further partition was implemented to obtain a balance between critical values and potential mis-ranked ROC curves. That is, we wanted to identify a number of segments that would correspond to a reasonable threshold value, given standard Type-I error probabilities. Such division was also performed to facilitate the computation of Spearman rank-order correlations for each film separately. We then used these rankings to compute SRCs among all 105 possible pairs of variables ($\frac{J(J-1)}{2}$).

3.5. *Step 2: Emotion Network: Efficiency of Signal Transmission*

Based on the SRCs, we obtained for each pair of variables—in each viewing order—an empirical distribution based on 50 values (i.e., for the 50 individuals in each group, except for 51 in one group). From here, a matrix $\mathcal{P}(h)$ can be derived for any given threshold value h. We derived one such matrix for each of the three viewing orders, denoted as $\mathcal{P}^{(A)}(h)$, $\mathcal{P}^{(B)}(h)$ and $\mathcal{P}^{(C)}(h)$, with a threshold value $h = 0.503$. These matrices are presented in Tables 2, 3, 4 (with variables listed in no particular order).

For each of these matrices, we built a stochastic network $\mathcal{SN}$ using each variable as a node and the probability of association between each pair of variables as the wirings among the nodes. To evaluate the wiring expectation between each pair of nodes, we conducted a Monte Carlo experiment for each of the three matrices $\mathcal{P}^{(A)}(0.503)$, $\mathcal{P}^{(B)}(0.503)$, and $\mathcal{P}^{(C)}(0.503)$. We considered the following conditions for this simulation:

1. Given a network $\mathcal{SN}$, $J(J-1)/2$ Bernoulli random variables are generated to establish wiring connections based on a $\mathcal{P}(h)$ matrix.
2. A signal starts from one randomly selected node and is transmitted to all immediate neighbors (defined by analytic Step 1) with time steps $= 1$.
3. If nodes remain without activation, the signal is then transmitted from all activated nodes to their own immediate neighbors, with one more step.
4. After transmitting a signal to all its immediate neighbors, a node becomes deactivated, unless it also receives a signal from other nodes.
5. Through an iterative procedure, signal transmission is performed until the system converges into one of three patterns: (a) all nodes are simultaneously activated (on), (b) all

TABLE 2.
Matrix $P(h)$ ($h = 0.503$) for Viewing Group A.

A/0.5	SP	DP	PA	EA	TF	SC	RD	AB	SB	ET	PT	PP	AC	HR	PR
SP	–	0.94	0.73	0.45	0.43	0.50	0.27	0.45	0.33	0.35	0.55	0.16	0.20	0.18	0.20
DP	–	–	0.63	0.55	0.47	0.44	0.16	0.33	0.29	0.24	0.37	0.18	0.18	0.21	0.22
PA	–	–	–	0.45	0.39	0.52	0.37	0.45	0.37	0.35	0.51	0.20	0.24	0.18	0.31
EA	–	–	–	–	0.33	0.21	0.27	0.37	0.35	0.18	0.22	0.14	0.22	0.22	0.14
TF	–	–	–	–	–	0.42	0.27	0.37	0.39	0.14	0.18	0.16	0.24	0.12	0.27
SC	–	–	–	–	–	–	0.44	0.65	0.63	0.35	0.29	0.29	0.42	0.25	0.23
RD	–	–	–	–	–	–	–	0.94	0.73	0.43	0.45	0.35	0.63	0.39	0.31
AB	–	–	–	–	–	–	–	–	0.78	0.43	0.53	0.35	0.61	0.33	0.27
SB	–	–	–	–	–	–	–	–	–	0.35	0.35	0.33	0.45	0.27	0.20
ET	–	–	–	–	–	–	–	–	–	–	0.65	0.57	0.39	0.24	0.41
PT	–	–	–	–	–	–	–	–	–	–	–	0.58	0.37	0.24	0.57
PP	–	–	–	–	–	–	–	–	–	–	–	–	0.33	0.14	0.45
AC	–	–	–	–	–	–	–	–	–	–	–	–	–	0.39	0.35
HR	–	–	–	–	–	–	–	–	–	–	–	–	–	–	0.43
PR	–	–	–	–	–	–	–	–	–	–	–	–	–	–	–

TABLE 3.
Matrix $P(h)$ ($h = 0.503$) for Viewing Group B.

B/0.5	SP	DP	PA	EA	TF	SC	RD	AB	SB	ET	PT	PP	AC	HR	PR
SP	–	0.88	0.73	0.50	0.42	0.38	0.21	0.44	0.29	0.29	0.58	0.13	0.15	0.10	0.13
DP	–	–	0.60	0.48	0.29	0.31	0.21	0.31	0.25	0.33	0.42	0.17	0.13	0.17	0.21
PA	–	–	–	0.50	0.29	0.40	0.21	0.35	0.29	0.29	0.48	0.08	0.22	0.21	0.13
EA	–	–	–	–	0.25	0.54	0.35	0.48	0.35	0.29	0.38	0.15	0.28	0.38	0.13
TF	–	–	–	–	–	0.31	0.25	0.33	0.31	0.31	0.21	0.21	0.24	0.19	0.29
SC	–	–	–	–	–	–	0.60	0.81	0.69	0.42	0.46	0.23	0.43	0.25	0.25
RD	–	–	–	–	–	–	–	0.83	0.71	0.38	0.38	0.25	0.57	0.29	0.23
AB	–	–	–	–	–	–	–	–	0.77	0.44	0.60	0.31	0.50	0.25	0.17
SB	–	–	–	–	–	–	–	–	–	0.23	0.35	0.13	0.30	0.25	0.13
ET	–	–	–	–	–	–	–	–	–	–	0.58	0.50	0.33	0.29	0.33
PT	–	–	–	–	–	–	–	–	–	–	–	0.56	0.48	0.33	0.44
PP	–	–	–	–	–	–	–	–	–	–	–	–	0.41	0.17	0.50
AC	–	–	–	–	–	–	–	–	–	–	–	–	–	0.43	0.37
HR	–	–	–	–	–	–	–	–	–	–	–	–	–	–	0.56
PR	–	–	–	–	–	–	–	–	–	–	–	–	–	–	–

TABLE 4.
Matrix $P(h)$ ($h = 0.503$) for Viewing Group C.

C/0.5	SP	DP	PA	EA	TF	SC	RD	AB	SB	ET	PT	PP	AC	HR	PR
SP	–	0.89	0.74	0.50	0.30	0.52	0.20	0.44	0.31	0.35	0.50	0.13	0.17	0.09	0.22
DP	–	–	0.57	0.57	0.26	0.42	0.19	0.31	0.24	0.24	0.35	0.19	0.13	0.13	0.33
PA	–	–	–	0.56	0.37	0.48	0.33	0.50	0.35	0.37	0.52	0.15	0.28	0.09	0.19
EA	–	–	–	–	0.35	0.40	0.30	0.52	0.35	0.15	0.24	0.22	0.20	0.15	0.22
TF	–	–	–	–	–	0.27	0.44	0.39	0.33	0.17	0.07	0.19	0.19	0.11	0.24
SC	–	–	–	–	–	–	0.37	0.60	0.42	0.38	0.40	0.23	0.33	0.10	0.15
RD	–	–	–	–	–	–	–	0.91	0.67	0.33	0.26	0.35	0.56	0.13	0.15
AB	–	–	–	–	–	–	–	–	0.70	0.41	0.50	0.31	0.50	0.07	0.17
SB	–	–	–	–	–	–	–	–	–	0.31	0.33	0.19	0.30	0.09	0.19
ET	–	–	–	–	–	–	–	–	–	–	0.54	0.59	0.31	0.13	0.37
PT	–	–	–	–	–	–	–	–	–	–	–	0.44	0.33	0.28	0.39
PP	–	–	–	–	–	–	–	–	–	–	–	–	0.24	0.11	0.44
AC	–	–	–	–	–	–	–	–	–	–	–	–	–	0.20	0.22
HR	–	–	–	–	–	–	–	–	–	–	–	–	–	–	0.59
PR	–	–	–	–	–	–	–	–	–	–	–	–	–	–	–

nodes are alternatively activated (on/off); and, (c) some nodes are never activated (i.e., isolated nodes).

In sum, a node can be switched "on" if the probability of association with its neighbor nodes exceeds a determined threshold. Given a signal on a neighbor variable, the node will likely be "on", whereas other nodes not strongly related will remain "off". At the next step, those variables that reach connection are allowed to connect with their neighbors (i.e., if strongly related), and so on. This conceptualization of signal transmission, as states in which nodes could be "on" and "off", was meant to follow the firing of neurons in the brain.

When all the nodes in the system become simultaneously activated (pattern (a)), the network is said to have achieved coherence. This system-wise coherence implies that all the signals are engaged in simultaneous amplitude and phase adjustments (i.e., a coordinated response by the signals to an intense stimulus). To create a network that allows multivariate coherence and can represent an emotion system, we need to regulate signal transmission within a node and then describe how amplitude-and-phase adjustments could be possible. Three properties are necessary for such a network to allow system-wise coherence: (a) all nodes in the network have the capability and tendency of returning to a "non-activated" state, (b) all nodes perform an amplitude-and-phase adjustment by simultaneously passing and receiving the signal; and, (c) all nodes are connected and are capable of performing a mutual amplitude-and-phase adjustment with their nearest neighbors. A system that satisfies these three conditions is a system capable of showing system-wise coherence. In order for such a system to be activated, a strong and persistent stimulus is needed. These criteria allow us to distinguish systems sensitive to system-wise coherence from those not capable of such coherence (see Appendix B for examples and mathematical details, and McAssey et al., 2010, for an in-depth discussion).

When a system achieves coherence, the number of steps needed to achieve such a state are counted. For this, we performed 10,000 replications of this process and recorded, for each replication, the proportion of nodes activated by the signal at each time step. A summary of these proportions, across all replications is depicted in Figure 6 (for viewing order A). This figure represents the distributions of increments in activated nodes for each signal transmission across four consecutive time steps. We denote this sequence as $\{D_i(\mathcal{P}^{(A)}(0.503))\}_{i=1}^{4}$. For example, the first distribution $D_1(\mathcal{P}(h))$ represents the distribution of immediately connected neighbors of any given node in the $\mathcal{SN}$ governed by the matrix $\mathcal{P}(h)$. In this case, this size is about eight. This is an important characteristic of $\mathcal{SN}$, which is similar to the average cluster size of a small-world network (see Watts & Strogatz, 1998). The second distribution $D_2(\mathcal{P}(h))$ represents the spread of network branching from the immediate neighbors of an initial node, which is about nine or ten in this case. The third and fourth distributions can be interpreted similarly, indicating that virtually all nodes in this system are activated after the second time step. With $\{D_i(\mathcal{P}(h))\}_{i=1}^{4}$ exhibiting system-wise characteristics of a network based on $\mathcal{P}(h)$) with a positive threshold h, we use this sequence of distributions to characterize coherence in the entire dynamic system.

3.6. Step 3: Hierarchical Clustering

In the next set of analyses, we examined the connecting structure underlying the 15 emotion variables. We investigated whether or not these variables are connected as a small-world network, with several clusters linked through stable wirings. We then examined, in probabilistic terms, whether this structure is conducive to robust signal transmission.

Consider the small-world network $\mathcal{SN}$ based on the matrix $\mathcal{P}^{(A)}(h)$. The probability $d(j, j') = 1 - \hat{p}(h|j, j')$ can be interpreted as a direct "distance" between j and j'. Using $d(\cdot, \cdot)$ as a metric, we performed hierarchical clustering analyses using the complete link method that resulted in clustering trees (or dendrograms), with corresponding distances among the variables. Results from these analyses are depicted in Figure 7, for the three viewing orders.

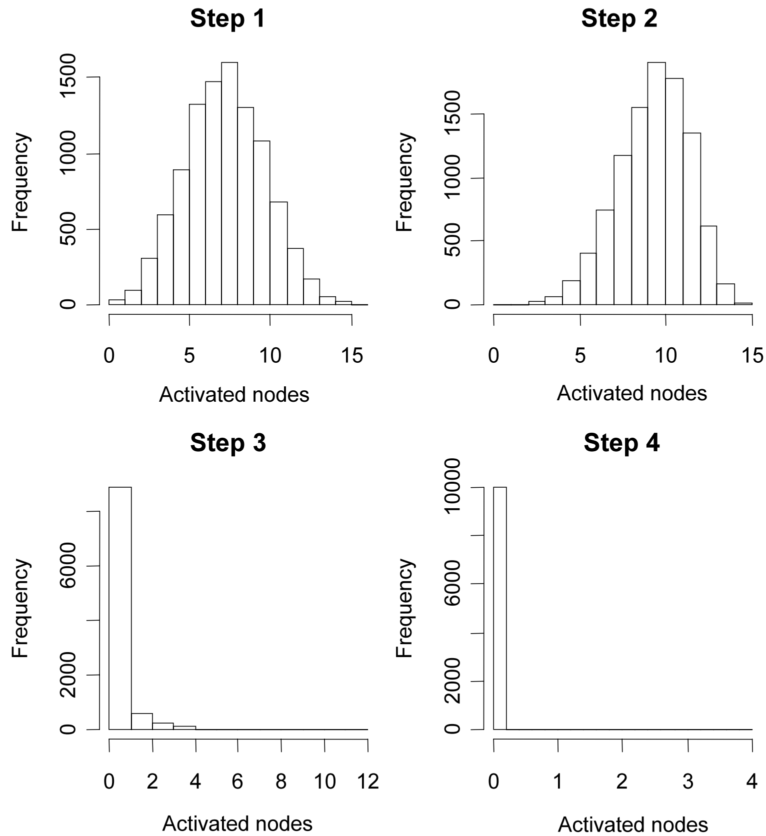

FIGURE 6.
Distributions of activated nodes during signal transmission at each time step (Viewing order A).

For clustering tree A, for example, three main branches are apparent. Each branch stems from a solid cluster with seemingly strong wirings. One core-cluster comprises blood pressure variables (i.e., systolic and diastolic, *SP* and *DP*). The two other core-clusters are related to cardiac activation (i.e., heart rate, total peripheral resistance, *HR* and *PR*) and related to experiential and behavioral emotion (i.e., rating dial, facial amusement and sadness, *RD*, *AB*, and *SB*). Within each branch, the wiring probability becomes smaller as the two nodes are further away from the core-cluster. The core-clusters in the trees for the viewing orders B and C have comparable structures.

In addition to the core-clusters, wiring is also possible both within and between branches, although the former is more likely. For example, between the "Blood-Pressure" and "Cardiac Activation" branches there are $5 \times 2 = 10$ (i.e., number of variables in each branch) possible wirings, 40 between the Blood-Pressure and Behavior branches, and 16 between the Cardiac and the Affective branches. We argue that all these potential wirings are redundant, as they do not affect the core structure of the network, and that deleting some of them does not affect the structure of the network, nor does it alter efficiency of signal transmission.

3.7. Step 4: Stochastic Networks Structure

The presence of core-clusters and redundant wirings is an important characteristic of small-world networks, for which we conclude that these variables are connected as a small-world network. The relevant feature here is the efficient signal transmission from one node to the entire

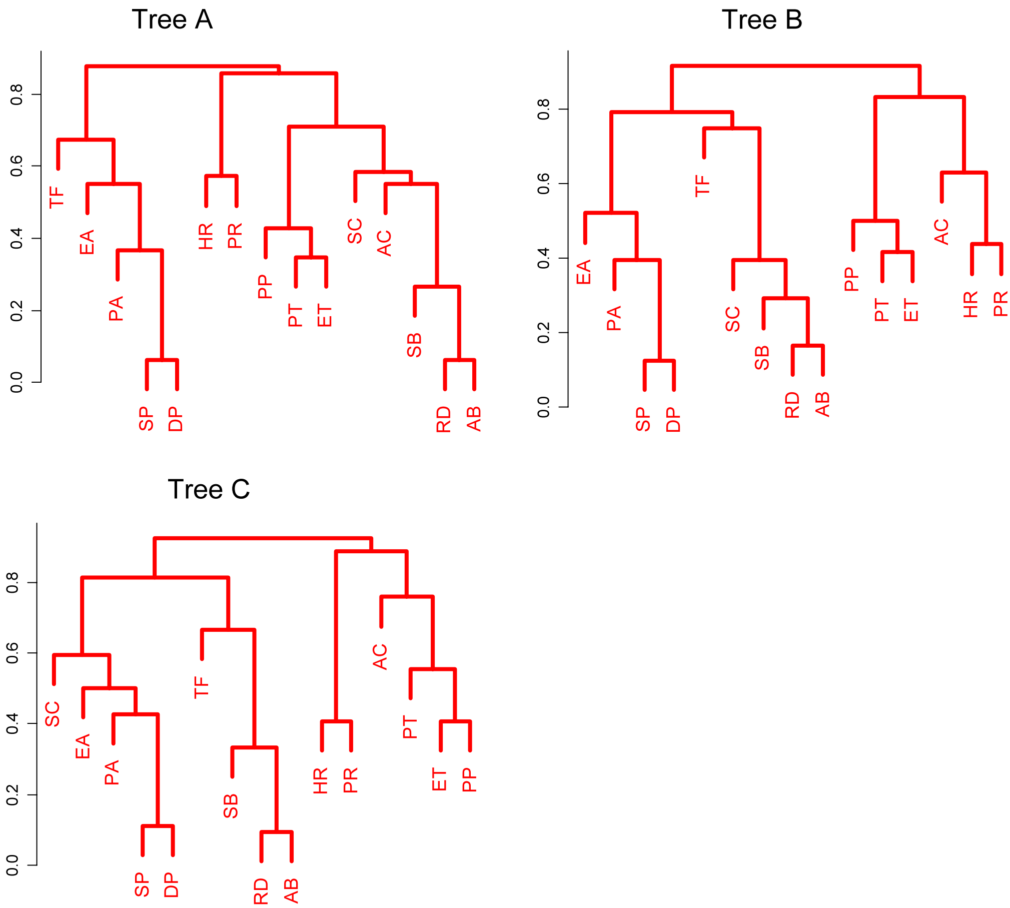

FIGURE 7.
Clustering trees of emotion variables (across viewing groups).

system. One possible argument for such redundancy is as follows: Suppose that a (j, j') pair of network nodes is connected. The conditional probability that this wiring is false is equal to the ratio $\frac{\alpha(h)}{\hat{p}(h|j,j')}$, for instance $\frac{\alpha(0.503)}{\hat{p}(0.503|j,j')} = \frac{0.05}{\hat{p}(0.503|j,j')}$. When $\hat{p}(0.503|j, j')$ is close to 1, then this conditional probability is rather small. Such small conditional probability will guarantee that an isolated node within the core-cluster is very unlikely to occur, with probability less than $(0.05)^2$, with $h = 0.503$, as the likelihood of observing false wirings is low.

On the other hand, this conditional probability would be significant only when $\hat{p}(h|j, j')$ is close to $\alpha(h)$. Again, with $h = 0.503$ and $\alpha(0.503) = 0.05$, the wiring based on the probability $\hat{p}(h|j, j') \approx 0.05$ would hardly occur in $\mathcal{SN}$, which suggests that if false wirings exist, they are more likely to occur between branches. This is because the group of wirings between branches $(10 + 40 + 16)$ occupies the majority of the total wiring in the network, as $(10 + 40 + 16)/105 = 66/105$, with $h = 0.503$.

Similarly, the expected number of false wirings is relatively small for a given h, say $h = 0.503$. Moreover, such false wiring is not likely to cluster all between one particular pair of branches. Hence, removing all false wirings from $\mathcal{SN}$ would have a negligible effect on the overall performance of the network. This argument is also informative for choosing the threshold parameter h. As demonstrated here, $h = 0.503$ is a reasonable choice that balances the number of potential false wiring and reveals the small-world structure of $\mathcal{SN}$ based on $\mathcal{P}^{(A)}(h)$. Similar structures are seen on $\mathcal{SN}$ based on $\mathcal{P}^{(B)}(0.503)$ and $\mathcal{P}^{(C)}(0.503)$.

3.8. Step 5: System-Wise Coherence Across Emotional Responses

As described previously, we use the sequence of distributions $\{D_i(\mathcal{P}(h))\}_{i=1}^4$ as exhibiting system-wise characteristics of a network based on $\mathcal{P}(h)$) with a positive threshold h, to characterize the efficiency of the network. Furthermore, based on these sequences, we compared different degrees of efficiency across different conditions. For example, here we compared efficiency across emotional stimuli of different valence. The goal of these comparisons is to evaluate the hypothesis that the amusement and sadness films elicit stronger signals than the neutral films. To answer this question, we performed a number of comparisons within each group. Given a threshold value 0.503, let $\mathcal{P}^{(A_1)}(h)$, $\mathcal{P}^{(A_2)}(h)$, $\mathcal{P}^{(A_3)}(h)$, and $\mathcal{P}^{(A_4)}(h)$ be matrices representing each of the four films for group A. Based on each of these four matrices, we conducted a Monte Carlo simulation with 10,000 replications to examine the efficiency of signal transmission in each of the segments. From this simulation, we obtained a sequence of distributions denoted as $\{D_i(\mathcal{P}^{(A_k)}(0.503))\}_{i=1}^4$ for $k = 1, 2, 3$, and 4, where i represents the index of time steps of signal traveling through the network and k represents each of the four segments in the films, and similar notations for viewing orders B and C.

For each of the three viewing orders, we then constructed four ROC curves (one for each emotional film—sad, neutral, amusing, and neutral) representing discrepancies between the distribution of transmission efficiency for each film and the entire series. We then compared the resulting efficiency from each of the four films. ROC curves with these comparisons are depicted in Figure 8. The results from these comparisons indicate that, across all viewing groups, the ROC curve from the amusing film was constantly the highest among all curves, suggesting the strongest coordination of responses and, thus, the most efficient signal transmission. In contrast, the second neutral film was constantly the lowest among the ROC curves, suggesting the least efficient signal transmission, also for all groups. Moreover, for group B, the sad film elicited responses similar to those in the amusing film, whereas for groups A and C, the first neutral film elicited responses similar to those in the amusing film. Overall, these results indicate that films with a strong emotional component induced greater coherence than neutral stimuli did.

Across all viewing orders, the ROC curves at the last signal transmission are almost straight lines and intersect the vertical line $t = 1$ at values less than 1 on the Y-axis. Being strictly less than 1 indicates that the network $\mathcal{SN}$ based on the entire series is much more efficient than the network based on any of the segments. ROC curves becoming straight lines, however, is an artifact of very concentrated distributions at 1. In the last set of analyses, we used these same procedures to compare the system-wise coherence across the different viewing orders. These analyses revealed similarity in signal efficiency and, thus, emotional coherence across viewing orders. Such similarities suggest a similar coordination in the patterns of emotion responses across the viewing groups.

4. Discussion: Methodological and Theoretical Implications

In this paper, we proposed an approach to examine coherence in a multivariate system based on the patterns of associations among all variables. We illustrated our method with empirical data from 15 experiential, behavioral, and physiological variables. Our analyses indicated that this group of variables had a typical small-world network structure (Watts & Strogatz, 1998), with three separate clusters and strong connections within each cluster. This structure had a large cluster size (i.e., many nodes were activated at the first time step) and a short path-length

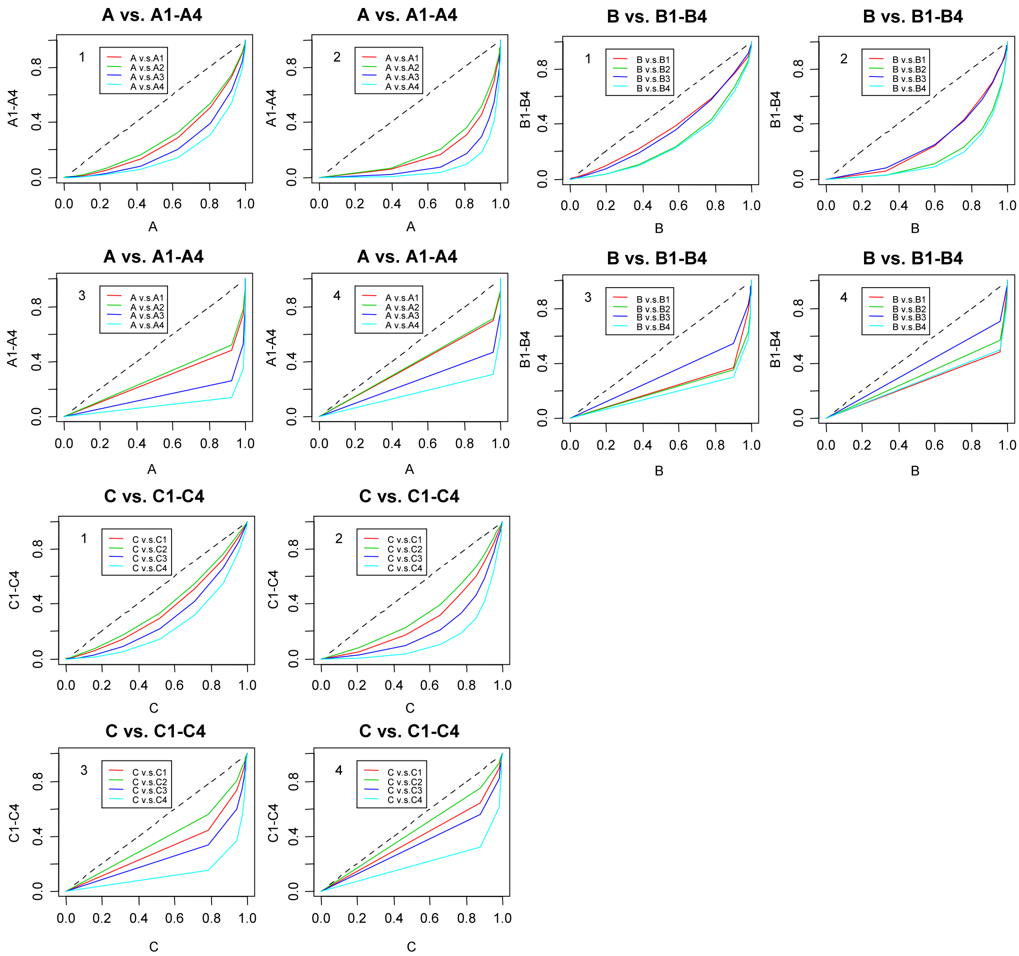

FIGURE 8.
ROC curves for comparing system-wise coherence across emotion stimuli. Colors correspond to the different films (*red* = amusement; *green* = neutral; *blue* = sadness; *cyan* = neutral).

(i.e., all nodes were activated at the second time step). Such configuration was conducive to effective signal transmission across the entire network. In other words, given a stimulus in any emotion variable of the system, all the emotion signals in the network would become quickly interconnected. When signal transmission was compared across experimental conditions, our results indicate that coherence was stronger for intense emotional stimuli than for neutral stimuli.

4.1. Methodological Considerations

Conceptualizing a multivariate system as a small-world network and evaluating coherence using all the variables in the system has several implications. First, this approach can provide information about the structure and dynamics of the system. The time steps in our method reflect the structure of association (i.e., coordination) among all the variables in the network. Given that such connections are based on a probability threshold, computed from all possible connections, these time steps represent the extent to which the variables in the system are connected. In this way, such network representation can be informative about the dynamics of the entire system, as it reveals the clusters of variables, the connections among such clusters, and the associations among the variables in the entire structure. A system that quickly reaches a stable configuration implies a quick coordination of responses; its structure is such that the variables are strongly connected, even if two given variables are loosely associated. The proposed stochastic networks relate to the original data in that they represent the associations—and their strength—among all the variables in the system.

A practical implication of our approach is that coherence can be assessed using signals measured in real time and with various time metrics. Each of the films in our data lasted for a certain period of time, thus imposing a given temporal resolution. Temporal resolution and timing of measures are indeed described as important factors that might affect indices of coherence among response systems (Mauss et al., 2005). This is especially the case when measuring emotion experience. Here, researchers have often relied on retrospective and aggregated ratings because it is difficult to assess emotional experience online and moment-by-moment without impeding emotion induction (e.g., Gottman & Levenson, 1985; Rosenberg & Ekman, 1994).

Our analyses assumed that all the individuals were randomly drawn from the same population. In particular, the $\mathcal{P}(h)$ matrices contain the proportion of people likely to have connections among variables. In this way, the generated networks could be thought as different individuals from that population, some of which have a particular connection between nodes, whereas others do not. There is a growing body of psychological literature questioning whether aggregates are useful descriptions of the individual (e.g., Hamaker, Dolan, & Molenaar, 2005; Molenaar, 2004; Nesselroade & Molenaar, 1999). Our ROC curve analyses were conducted at the individual level and this information was then compiled in all subsequent analytic steps. Although perhaps not an optimal approach, our analyses were built upon individual information.

There is much work in the areas of time series, nonlinear dynamics, information theory, and neuroscience dealing with synchronization (Pikovsky, Rosenblum, & Kurths, 2001) and coherence in multivariate systems (e.g., Quian Quiroga, Kraskov, Kreuz, & Grassberger, 2002). One example of such work are the measures of higher-order mutual information such as the Kullback–Leibler divergence (see Schneidman, Still, Berry, & Bialek, 2003; Klinkner, Shalizi, & Camperi, 2006). Although these can be highly informative approaches, we believe that our focus has unique features and is particularly relevant to our data and research question.

Finally, in our analyses of pairwise coherence, we used SRCs as a nonparametric approach that is robust under conditions of varying measurement units and waveforms. We compared this approach with standard cross-correlations and found that, under conditions of non-stationarity, especially data with periods that vary in important signal features (i.e., wave-length), SRCs can better capture the associations among variables. Specifically, cross-correlations in the simulation were consistently smaller than SRCs, especially under large noise. Comparisons using empirical data yielded similar results. Full details of these comparisons are included in Appendix A.

4.2. Limitations and Future Directions

Our main goal in this report was to characterize coherence as a system-wise measure. We did this by examining whether or not a number of different time series were driven by some coherent process. One aspect that we did not investigate, however, was whether coherence was produced by a single or several processes. It would be possible to find instances in which all variables are interrelated but without a unified coherent process underlying the pattern of correlations (see, e.g., van der Maas, Dolan, Grasman, Wicherts, Huizenga, & Raijmakers, 2006).

Our analyses were primarily data driven. This was particularly reflected in two steps of our analyses: the random selection of nodes for signal transmission, and the use of empirical probabilities as the wiring structure in the network. These criteria, however, could be changed to accommodate specific hypotheses. For example, one might want to determine whether signal transmission follows a hypothetical order and choose the starting node accordingly. Similarly, the network structure could be specified based on theory, instead of on the empirical probabilities.

One such theoretical configuration could predict strong connections among all the physiological variables, all the experiential variables, and all the behavioral variables, with weaker connections among the three clusters (see, e.g., Network B in Figure 4). This would represent an emotion network that integrates three interconnected subsystems, and coherence would point to three distinct—yet coordinated—processes. This network could then be compared with the hypothesis of a single process driving coherence (e.g., all the nodes are similarly connected, as in Network A in Figure 4). Such an approach would allow the evaluation of specific models of emotion, with potential implications for hypothesis testing as well as theory building.

Comparing among alternative specifications could be used to identify redundant nodes in the network and determine parsimonious structures. For example, the association between finger pulse amplitude and the two blood pressure variables in our data are large (i.e., 0.73 and 0.63; see Table 2). Although specifying a network with a low probability of connections among these variables does not appear reasonable, signal transmission in such a model could be compared with that from the empirical data, along the lines of covariance structure analysis. Similarly, finger temperature and pre-ejection period (i.e., TF, PP) appear to be weakly connected with some other variables (Tables 2–4). Such variables could be removed from the network and the resulting structure evaluated for signal transmission. These extensions have important implications and deserve a detailed examination that goes beyond the scope of our article.

4.3. *Implications for Affective Science*

We examined coherence in terms of coordination of emotion responses. Although emotion theories describe coherence as a defining feature of emotion systems (e.g., Ekman 1972, 1992; Lazarus, 1991; Levenson 1994, 2003; Matsumoto et al., 2007; Scherer, 1984; Tomkins, 1962), coherence across multiple variables is still largely an unanswered question. Our approach adds to previous research by extending bivariate analyses to multivariate systems.

Our conceptualization of emotion coherence was as a concordance of phases across all the responses along the different stimuli. Two features are necessary for this system-wise coherence: synchrony of phases at any time point and maintenance of such concordance along the trajectory of the stimuli. From the standpoint of affective theory, this conceptualization implies the coordination of all substructures (e.g., experiential, behavioral, and physiological) that are part of an individual's affective system. In response to an emotional stimulus, such substructures would get activated and coordinated, after which they would follow an interrelated pattern, very much like a school of fish, as the emotion unfolds over time. Although represented in theories of emotion, these features are not currently present in empirical emotion research.

Several of our findings have implications for emotion theory. They relate to the question, do emotionally charged stimuli elicit different coherence than neutral stimuli? Our comparisons among the segments indicate stronger coherence during positive and negative emotional states. This finding supports the notion that emotional—compared to neutral—states engender system coherence. Such coherence, however, might be a function of valence (positive-negative) rather than discrete emotional states (cf. Feldman-Barrett, 2006). Furthermore, we found uniform results across the different viewing orders, implying generalizability of our findings and, thus, emotional coherence. We also found differences between the amusing and sad films. For most individuals, the responses to the amusing film appeared and dissipated quickly. The responses to the sad film, however, were delayed for many individuals, and such responses lingered through the next segment. This finding points to possible time differences between positive and negative emotions. Whereas the former have quicker time-course, the latter seem to linger (e.g., Ferrer & Nesselroade, 2003).

With regard to the network configuration of the data, our findings indicate the existence of three clusters: blood pressure, cardiac activation, and behavioral variables. This suggests that, within the overall system, there are subsystems with relatively greater coherence. This network has a typical small-world structure, with large cluster size and short path-length, which is effective for transferring and processing information throughout the network. In our data, only two steps were required to transmit a signal across all nodes and associate the entire network. In other words, the shortest distance of any pair of nodes was no more than two steps. An important implication of this small-world structure is that any given pair of variables will connect very rapidly, even if they are weakly related and located on separate clusters. For example, the association between heart rate and finger temperature is 0.12 (Table 2), and they are located in different clusters (Figure 7, Tree A). In spite of this, the coherence across the entire system is such that these two variables are strongly connected through the network.

4.4. Concluding Comments

In sum, in this manuscript we present an approach to examine system-wise coherence among multiple time-varying responses. This is a flexible approach that uses small-world networks and signal transmission based on the interrelations among variables. We illustrate the utility of this method with psychophysiological data. We hope that this approach opens new possibilities for studying coherence in multivariate dynamic systems.

Acknowledgements

We thank Michael McAssey for his help with the computation of signal transmission.

Appendix A

A.1. Spearman Rank Correlations and Cross-Correlations: Simulation Study

The cross-correlation function (CCF) between any two time series, namely $\{x_s\}_{s=1}^N$ and $\{y_t\}_{t=1}^N$, at time points (s,t) is, in general, defined as

$$\rho_{xy}(s,t) = \frac{\gamma_{xy}(s,t)}{\sqrt{\gamma_x(s,s)\gamma_y(t,t)}}, \quad \text{with} \tag{A.1}$$

$$\gamma_{xy}(s,t) = E\big[(x_s - \mu_{xs})(y_t - \mu_{yt})\big] \tag{A.2}$$

where $\mu_{xs} = E[x_s]$ and $\mu_{yt} = E[y_t]$.

The above definition does not involve any assumption regarding stationarity (i.e., no changes in the distribution of means or variances with respect to time).[5] In most cases, however, the two time series are the only available data. Therefore, neither μ_{xs} nor μ_{yt} are known, nor are the variances $\gamma_x(s,s)$ and $\gamma_y(t,t)$, or the covariance $\gamma_{xy}(s,t)$.

When stationarity can be assumed for both time series, these parameters can be estimated by simple averages and, more importantly, $\rho_{xy}(s,t) = \rho_{xy}(s', s'|t-s|) = \rho_{xy}(|t-s|)$ for all s'. That is, denote $h = |t-s|$, then

$$\hat{\rho}_{xy}(h) = \frac{\hat{\gamma}_{xy}(h)}{\sqrt{\hat{\gamma}_x(0)\hat{\gamma}_y(0)}}, \quad \text{with} \tag{A.3}$$

$$\hat{\gamma}_{xy}(h) = \sum_{s'=1}^{N-h} \big[(x_{s'} - \bar{x})(y_{s'+h} - \bar{y})\big]/N \tag{A.4}$$

where $\bar{x} = \sum x_s/N$ and $\bar{y} = \sum y_t/N$.

[5] More formally, a time series $X_1, X_2, \ldots, X_N$ is non-stationary if, for some m, the joint probability distribution of the m-vector $X_{i+1}, X_{i+2}, \ldots, X_{i+m}$ is dependent on the time index i (see Priestley, 1988).

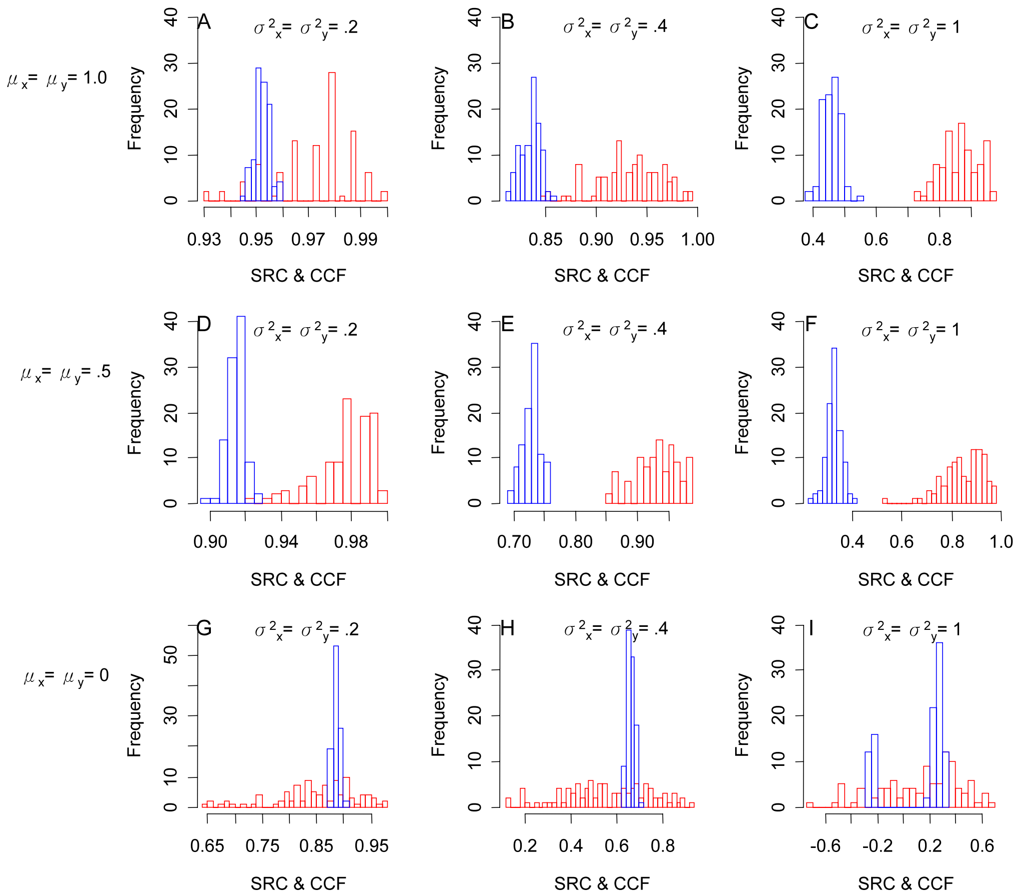

FIGURE 9.
Histograms of CCF (*red*) and SRC (*blue*) from simulations.

When departure from stationarity is large, the overall averages $\bar{x}$ and $\bar{y}$ will differ from μ_{xs} and μ_{yt} for any time point s and t. Moreover, the calculated cross-correlation may not capture important information regarding the linear relationship between both variables. To examine this limitation of cross-correlation and its use to infer coherence, we performed a simulation study in which we compare cross-correlations and Spearman correlations as approaches to capture relationship between two variables.

The simulation setting is as follows. Consider the following signal conditions, $S(t_i)$ as

$$\begin{cases} S(t_i) = \sin(2\pi \frac{t_i}{15}) \times 1 + \mu, & 1 \le t_i \le 150; \\ S(t_i) = \sin(2\pi \frac{t_i}{30}) \times 0.5 + 0, & 151 \le t_i \le 300; \\ S(t_i) = \sin(2\pi \frac{t_i}{15}) \times 1 - \mu, & 301 \le t_i \le 450; \\ S(t_i) = \sin(2\pi \frac{t_i}{30}) \times 0.5 + 0, & 451 \le t_i \le 600. \end{cases}$$

Consider now two series, $X(t_i)$ and $Y(t_i)$, sharing the same signal and with independent measurement error, such that $X(t_i) = S(t_i) + e_{x(t_i)}$ and $Y(t_i) = S(t_i) + e_{y(t_i)}$. Moreover, $e_x(t_i) \sim \text{Normal}(0, \sigma^2)$ and $e_y(t_i) \sim \text{Normal}(0, \sigma^2)$, and $\sigma^2_{ex} = \sigma^2_{ey}$, with $\rho_{ex,ey} = 0$.

To compare the cross-correlations with Spearman correlations across different data conditions, we included three parameter values for $\sigma^2 = 0.2$, 0.4, and 1, as well as three parameter

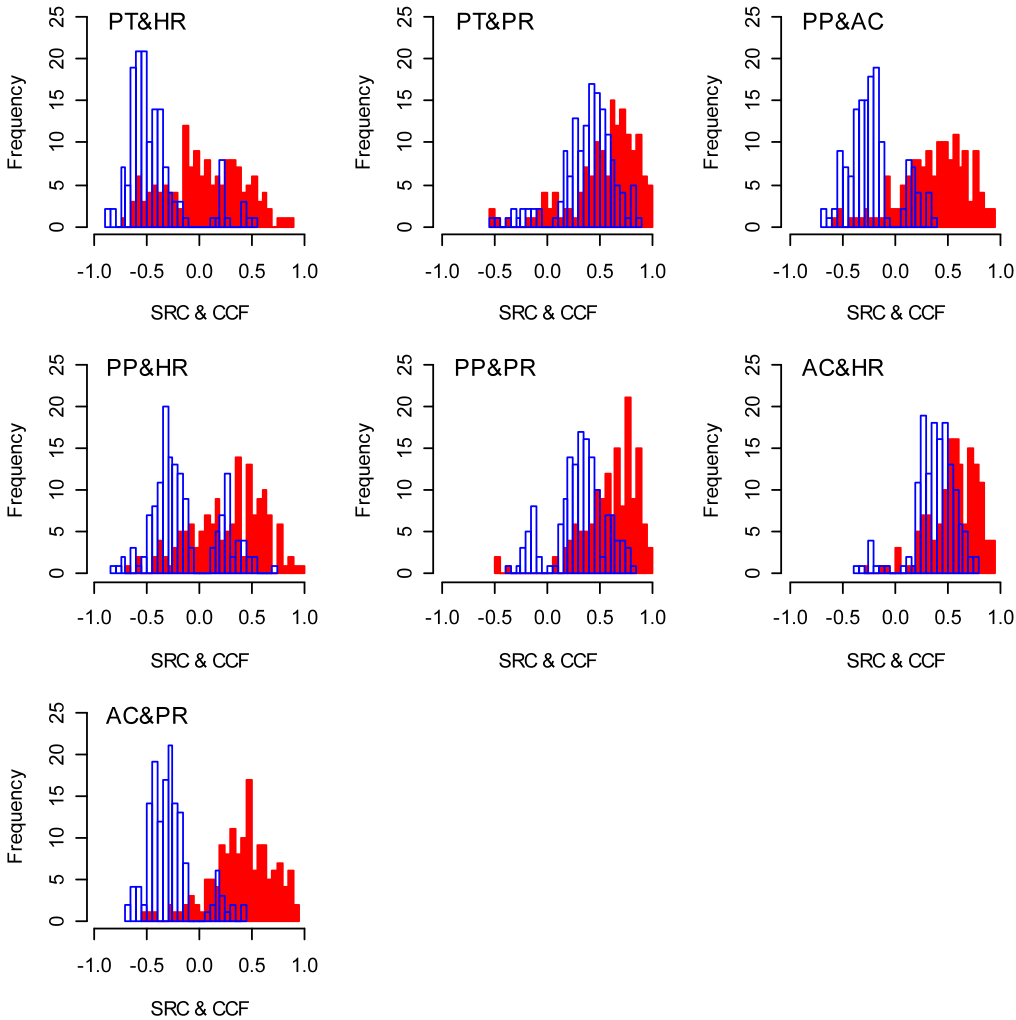

FIGURE 10.
Histograms of CCF (*red*) and SRC (*blue*) from empirical data.

values for the constant $\mu = 1$, 0.5, and 0. Furthermore, the length of the time series is 600 (i.e., same as in the empirical data, to be described below), which was then partitioned into 12 segments (i.e., also in line with the empirical data).

The results of the simulation are depicted in Figure 9. The different panels in this figure represent the frequency distributions of values for CCF (lag 0) and Spearman rank correlations (SRCs) for the different conditions. Panels A–C depict the distributions of correlations under conditions of constant $\mu = 1$ (for both variables) with $\sigma^2 = 0.2$, 0.4, and 1 (Panels A–C, respectively). Panels D–F shows such distributions for conditions of $\mu = 0.5$ and $\sigma^2 = 0.2$, 0.4, and 1. Finally, the distributions in Panels G–I are those under conditions of $\mu = 0$ and $\sigma^2 = 0.2$, 0.4, and 1.

Results from a unit constant ($\mu = 1$) indicate that, irrespective of the noise, the CCFs tend to be smaller in magnitude than those of the SRCs, and this appears to be more marked for higher noise values. When the constant in both series decreases ($\mu = 0.5$ and 0, Panels D–I), the signal in the series comes primarily (or exclusively) from the different sine waves across the four periods. The results in these cases make the differences between CCFs and SRCs more evident, especially for larger noise and, in particular, for conditions of zero constant. Here, the distribution of the CCFs becomes bimodal, which is an undesirable property.

In sum, the results from this simulation indicate that CCFs did not capture the common signal relationship between both variables in the same way that SRCs did. A fundamental reason for this discrepancy was because independent noise was added to the simulated data. Such data had four segments and the noise distorted the different sine waves. Under these conditions, CCFs did not fully depict the associations between both variables. The SRCs, in contrast, considered the different segments (and subsegments) and thus were able to represent the relationship between both variables more accurately.

A.2. *Spearman Rank Correlations and Cross-Correlations: Comparison with Empirical Data*

To illustrate possible differences between results obtained with CCFs and SRCs we now compare the distributions of both functions with empirical data. For this, we chose several pairs of variables. The frequency distributions from both correlations are depicted in Figure 10. For all pairs of variables, the CCFs (in blue, to the left) are of smaller magnitude than the SRCs (in red, to the right). For some of these pairs of variables (e.g., “finger pulse transit time” and “total peripheral resistance”) the differences are not very large but for most of them (e.g., “somatic activity” and “pre-ejection period”) the differences are very large with also discrepancy in the valence. These comparisons are in line with the results from our simulation and indicate that, under these data conditions and with clear non-stationarity, SRCs are a more reasonable choice than CCFs.

Appendix B

B.1. *Linear Algebraic Representation of a Network and Its Signal Transmission*

In this Appendix, we provide linear algebraic representations for a network and its signal transmission. We also mathematically define when a network can and cannot achieve system-wise coherence during its signal processing. We illustrate these linear algebraic representations using some of the networks displayed in Figure 4.

A network having 9 nodes (as in Figure 4) can be represented by a symmetric 9×9 matrix with 0–1 entries, say $\mathcal{N}$, with zeros on the main diagonal, i.e., $\mathcal{N}(ii) = 0,\ \forall i = 1, \ldots, 9$, and either $\mathcal{N}(ij) = 1$ or $\mathcal{N}(ij) = 0$ in the off-diagonal, where the (i, j)th entry represents a wiring between the ith and jth nodes. Therefore, Networks A and B can be represented by matrices $\mathcal{N}_A$ and $\mathcal{N}_B$ as in Figure 11.

Signal transmission within a network $\mathcal{N}$ is represented via the operation of multiplication. Let $e_i = (0, \ldots, 0, 1, 0, \ldots, 0)$ be the ith 9×1 vector in the Euclidean basis in $\mathbb{R}^9$. Here $v_0 = e_i$ stands for a signal initiated at the ith node. From the ith node, the signal is transmitted within the network to those nodes linked to the ith node, that is, to those non-zero entries in the ith row, $\mathcal{N}[i : \cdot]$, of $\mathcal{N}$. This signal transmission can be computed via matrix multiplication as $v_0^T \mathcal{N} = \mathcal{N}[i : \cdot] = v_1$. Here it is noted that $\mathcal{N}(ii) = 0$ means that the ith node sends the signal out to those nodes to which it is directly linked and then becomes deactivated. Under this pattern of signal transmission, we require that a node becomes activated only when it receives a signal from other nodes.

Further processing of the signal transmission can be concisely computed via the following indicator function: $V = \Im[U]$, which means that the vector V is the vector with 1s corresponding to the non-zero entries of vector U and 0s otherwise. With such a signal processing function, we

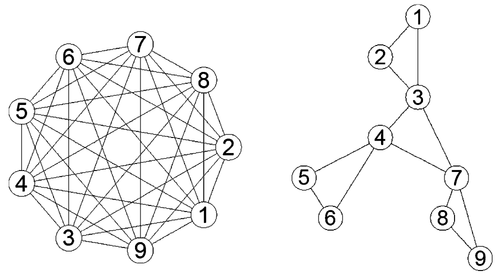

$$\mathcal{N}_A = \begin{bmatrix} 0&1&1&1&1&1&1&1&1\\ 1&0&1&1&1&1&1&1&1\\ 1&1&0&1&1&1&1&1&1\\ 1&1&1&0&1&1&1&1&1\\ 1&1&1&1&0&1&1&1&1\\ 1&1&1&1&1&0&1&1&1\\ 1&1&1&1&1&1&0&1&1\\ 1&1&1&1&1&1&1&0&1\\ 1&1&1&1&1&1&1&1&0 \end{bmatrix}, \qquad \mathcal{N}_B = \begin{bmatrix} 0&1&1&0&0&0&0&0&0\\ 1&0&1&0&0&0&0&0&0\\ 1&1&0&1&0&0&1&0&0\\ 0&0&1&0&1&1&1&0&0\\ 0&0&0&1&0&1&0&0&0\\ 0&0&0&1&1&0&0&0&0\\ 0&0&1&1&0&0&0&1&1\\ 0&0&0&0&0&0&1&0&1\\ 0&0&0&0&0&0&1&1&0 \end{bmatrix}$$

FIGURE 11.
Networks A and B.

$$\begin{bmatrix}1\\0\\0\\0\\0\\0\\0\\0\\0\end{bmatrix} \to \begin{bmatrix}0\\1\\1\\1\\1\\1\\1\\1\\1\end{bmatrix} \to \begin{bmatrix}1\\1\\1\\1\\1\\1\\1\\1\\1\end{bmatrix} \to \begin{bmatrix}1\\1\\1\\1\\1\\1\\1\\1\\1\end{bmatrix} \to \cdots$$

(a)

$$\begin{bmatrix}1\\0\\0\\0\\0\\0\\0\\0\\0\end{bmatrix} \to \begin{bmatrix}0\\1\\1\\0\\0\\0\\0\\0\\0\end{bmatrix} \to \begin{bmatrix}1\\1\\1\\1\\0\\0\\1\\0\\0\end{bmatrix} \to \begin{bmatrix}1\\1\\1\\1\\1\\1\\1\\1\\1\end{bmatrix} \to \begin{bmatrix}1\\1\\1\\1\\1\\1\\1\\1\\1\end{bmatrix} \to \cdots$$

(b)

FIGURE 12.
(**a**) Signal processing for Network A, with $v_0 = e_1$. (**b**) Signal processing for Network B, with $v_0 = e_1$.

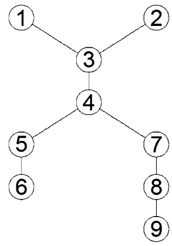

$$\mathcal{N}_E = \begin{bmatrix} 0 & 0 & 1 & 0 & 0 & 0 & 0 & 0 & 0 \\ 0 & 0 & 1 & 0 & 0 & 0 & 0 & 0 & 0 \\ 1 & 1 & 0 & 1 & 0 & 0 & 0 & 0 & 0 \\ 0 & 0 & 1 & 0 & 1 & 0 & 1 & 0 & 0 \\ 0 & 0 & 0 & 1 & 0 & 1 & 0 & 0 & 0 \\ 0 & 0 & 0 & 0 & 1 & 0 & 0 & 0 & 0 \\ 0 & 0 & 0 & 1 & 0 & 0 & 0 & 1 & 0 \\ 0 & 0 & 0 & 0 & 0 & 0 & 1 & 0 & 1 \\ 0 & 0 & 0 & 0 & 0 & 0 & 0 & 1 & 0 \end{bmatrix}$$

(a)

$$\begin{bmatrix}1\\0\\0\\0\\0\\0\\0\\0\\0\end{bmatrix} \to \begin{bmatrix}0\\0\\1\\0\\0\\0\\0\\0\\0\end{bmatrix} \to \begin{bmatrix}1\\1\\0\\1\\0\\0\\0\\0\\0\end{bmatrix} \to \begin{bmatrix}0\\0\\1\\0\\1\\0\\1\\0\\0\end{bmatrix} \to \begin{bmatrix}1\\1\\0\\1\\0\\1\\0\\1\\0\end{bmatrix} \to \begin{bmatrix}0\\0\\1\\0\\1\\0\\1\\0\\1\end{bmatrix} \to \cdots \to \begin{bmatrix}1\\1\\0\\1\\0\\1\\0\\1\\0\end{bmatrix} \to \begin{bmatrix}0\\0\\1\\0\\1\\0\\1\\0\\1\end{bmatrix} \to \cdots$$

(b)

FIGURE 13.
(**a**) Network E. (**b**) Signal processing for Network E, with $v_0 = e_1$.

obtain the kth transmission $v_k = \Im[v_{k-1}^T \mathcal{N}]$ from the $(k-1)$st transmission. Figure 12 reports the signal processing of Networks A and B.

From Figure 12, we see that Network A only requires two signal transmissions to produce a one-vector $1_{[9]} = (1, 1, \dots, 1)$, while Network B requires three signal transmissions to reach the same one-vector $1_{[9]}$. This one-vector $1_{[9]}$ indicates that all 9 nodes receive the signal and become simultaneously activated from then on. This is the state in which all nodes send out the signal and remain activated; equivalently, $1_{[9]} = \Im[1_{[9]}^T \mathcal{N}]$. We term this the state of system-wise coherence.

This state is not achievable by all networks. For example, Network D in Figure 3 can achieve system-wise coherence. However, if the wiring between nodes 3 and 7 is removed, the resulting network becomes a serial-type of network, denoted as Network E in Figure 13 of this Appendix. Even though all of its nodes are connected, Network E in Figure 13 is not capable of achieving system-wise coherence. In fact, eventually every node switches on-and-off alternately, never converging to a state of simultaneous activation.

References

Albert, R., Jeong, H., & Barabási, A.-L. (1999). Diameter of the world–wide web. *Nature*, *401*, 130–131.

Amaral, L.A.N., Diaz–Guilera, A., Moreira, A.A., Goldberger, A.L., & Lipsitz, L.A. (2004). Emergence of complex dynamics in a simple model of signaling network. *Proceedings of the National Academy of Sciences*, *101*, 155551–155555.

Boker, S.M., Xu, M., Rotondo, J.L., & King, K. (2002). Windowed cross-correlation and peak picking for the analysis of variability in the association between behavioral time series. *Psychological Methods*, *7*, 338–355.

Brillinger, D.R. (2001). Does anyone know when the correlation coefficient is useful? A study of the times of extreme river flows. *Technometrics*, *43*, 266–273.

Browne, M.W., & Nesselroade, J.R. (2005). Representing psychological processes with dynamic factor models: some promising uses and extensions of ARMA time series models. In A. Maydeu-Olivares & J.J. McArdle (Eds.), *Advances in psychometrics: a Festschrift to Roderick P. McDonald* (pp. 415–451). Mahwah: Erlbaum.
Cattell, R.B., Cattell, A.K.S., & Rhymer, R.M. (1947). P-technique demonstrated in determining psychophysical source traits in a normal individual. *Psychometrika*, *12*, 267–288.
Ekman, P. (1972). Universals and cultural differences in facial expressions of emotion. In J. Cole (Ed.), *Nebraska symposium on motivation* (pp. 207–282). Lincoln: University of Nebraska Press.
Ekman, P. (1992). An argument for basic emotions. *Cognition and Emotion*, *6*, 169–200.
Ekman, P., & Friesen, W.V. (1978). *The facial action coding system*. Palo Alto: Consulting Psychologists Press.
Feldman-Barrett, L. (2006). Are emotions natural kinds? *Perspectives in Psychological Science*, *1*, 28–58.
Ferrer, E., & Nesselroade, J.R. (2003). Modeling affective processes in dyadic relations via dynamic factor analysis. *Emotion*, *3*, 344–360.
Gottman, J.M. (1990). Time-series analysis applied to physiological data. In J.T. Cacioppo & L.G. Tassinary (Eds.), *Principles of psychophysiology: physical, social, and inferential elements* (pp. 754–774). New York: Cambridge University Press.
Gottman, J.M., & Levenson, R.W. (1985). A valid procedure for obtaining self-report of affect in marital interaction. *Journal of Consulting and Clinical Psychology*, *53*, 151–160.
Hamaker, E.L., Dolan, C.V., & Molenaar, P.C.M. (2005). Statistical modeling of the individual: rationale and application of multivariate stationary time series analysis. *Multivariate Behavioral Research*, *40*, 207–233.
Hastie, T., Tibshirani, R., & Friedman, J. (2009). *The elements of statistical learning* (2nd ed.). New York: Springer.
Hsieh, F., & Turnbull, B.W. (1996). Non- and semi-parametric estimation of the receiver operating characteristics (ROC) curve. *Annals of Statistics*, *24*, 25–40.
Johnson, S.C. (1967). Hierarchical clustering schemes. *Psychometrika*, *32*, 241–254.
Klinkner, K.L., Shalizi, C.R., & Camperi, M.F. (2006). Measuring shared information and coordinated activity in neuronal networks. In Y. Weiss, B. Scholkopf, & J.C. Platt (Eds.), *Advances in neural information processing systems* (pp. 667–674). Cambridge: MIT Press.
Lazarus, R.S. (1991). *Emotion and adaptation*. London: Oxford University Press.
Levenson, R.W. (1994). Human emotions: a functional view. In P. Ekman & R.J. Davidson (Eds.), *The nature of emotion: fundamental questions* (pp. 123–126). New York: Oxford University Press.
Levenson, R.W. (2003). Blood, sweat, and fears: the autonomic architecture of emotion. In P. Ekman, J.J. Campos, R.J. Davidson, & F.B.M. de Waal (Eds.), *Emotions inside out* (pp. 348–366). New York: The New York Academy of Sciences.
Levenson, R.W., & Gottman, J.M. (1983). Marital interaction: physiological linkage and affective exchange. *Journal of Personality and Social Psychology*, *45*, 587–597.
Matsumoto, D., Nezlek, J.B., & Koopmann, B. (2007). Evidence for universality in phenomenological emotion response system coherence. *Emotion*, *7*, 57–67.
Mauss, I.B., Evers, C., Wilhelm, F.H., & Gross, J.J. (2006). How to bite your tongue without blowing your top: implicit evaluation of emotion regulation predicts affective responding to anger provocation. *Personality and Social Psychology Bulletin*, *32*, 389–602.
Mauss, I.B., Levenson, R.W., McCarter, L., Wilhelm, F.H., & Gross, J.J. (2005). The tie that binds? Coherence among emotional experience, behavior, and autonomic physiology. *Emotion*, *5*, 175–190.
McAssey, M., Hsieh, F., & Ferrer, E. (2010). Optimal and robust design for efficient system-wide synchronization in networks of randomly-wired neuron-nodes. *Statistics and Its Interface*, *3*, 159–168.
Milgram, S. (1967). The small world problem. *Psychology Today*, *2*, 60–67.
Molenaar, P.C.M. (2004). A manifesto on psychology as idiographic science: bringing the person back into scientific psychology—this time forever. *Measurement*, *2*, 201–218.
Nesselroade, J.R., & Molenaar, P.C.M. (1999). Pooling lagged covariance structures based on short, multivariate time-series for dynamic factor analysis. In R.H. Hoyle (Ed.), *Statistical strategies for small sample research* (pp. 224–251). Newbury Park: Sage.
Pikovsky, A., Rosenblum, M., & Kurths, J. (2001). *Synchronization: a universal concept in nonlinear sciences*. Cambridge: Cambridge University Press.
Priestley, M.B. (1988). *Nonlinear and non-stationary time series*. New York: Academic Press.
Quian Quiroga, R., Kraskov, A., Kreuz, T., & Grassberger, P. (2002). Performance of different synchronization measures in real data: a case study on electroencephalographic signals. *Physical Review E*, *65*, 041903-14.
Rohatgi, V.K. (1984). *Statistical inference*. Mineola: Dover Publications.
Rosenberg, E.L., & Ekman, P. (1994). Coherence between expressive and experiential systems in emotion. *Cognition & Emotion*, *8*, 201–229.
Rottenberg, J., Ray, R.R., & Gross, J.J. (2007). Emotion elicitation using films. In J.A. Coan & J.J.B. Allen (Eds.), *The handbook of emotion elicitation and assessment* (pp. 9–28). New York: Oxford University Press.
Scherer, K.R. (1984). On the nature and function of emotion: a component process approach. In K.R. Scherer & P. Ekman (Eds.), *Approaches to emotion* (pp. 293–317). Hillsdale: Erlbaum.
Schneidman, E., Still, S., Berry, M.J., & Bialek, W. (2003). Network information and connected correlations. *Physical Review Letters*, *91*, 238701-4.
Swets, J.A. (1996). *Signal detection theory and ROC analysis in psychology and diagnostics: collected papers*. Mahwah: Erlbaum.
Tomkins, S.S. (1962). *Affect, imagery, consciousness: I. The positive affects*. Oxford: Springer.

Tsonis, P.A., & Tsonis, A.A. (2004). A "small-world" network hypothesis for memory and dreams. *Perspectives in Biology and Medicine*, *47*, 176–180.
van der Maas, H.L.J., Dolan, C.V., Grasman, R.P.P., Wicherts, J.M., Huizenga, H.M., & Raijmakers, M.E.J. (2006). A dynamical model of general intelligence: the positive manifold of intelligence by mutualism. *Psychological Review*, *113*, 842–861.
Watts, D.J., & Strogatz, S.H. (1998). Collective dynamics of 'small-world' networks. *Nature*, *393*, 440–442.
Watts, D.J. (1999). *Small worlds: the dynamics of networks between order and randomness*. Princeton: Princeton University Press.

Manuscript Received: 29 AUG 2008
Final Version Received: 26 MAY 2010
Published Online Date: 21 DEC 2010